Improvements to a model of projectile fragmentation

S. Mallik,[1] G. Chaudhuri,[1] and S. Das Gupta[2]
[1]*Variable Energy Cyclotron Centre, 1/AF Bidhannagar, Kolkata 700064, India*
[2]*Physics Department, McGill University, Montréal, Canada H3A 2T8*
(Received 29 August 2011; published 17 November 2011)

In a recent paper [Phys. Rev. C **83**, 044612 (2011)] we proposed a model for calculating cross sections of various reaction products which arise from disintegration of projectile-like fragments resulting from heavy-ion collisions at intermediate or higher energy. The model has three parts: (1) abrasion, (2) disintegration of the hot abraded projectile-like fragment (PLF) into nucleons and primary composites using a model of equilibrium statistical mechanics, and (3) possible evaporation of hot primary composites. It was assumed that the PLF resulting from abrasion has one temperature T. Data suggested that, while just one value of T seemed adequate for most cross-section calculations, a single value failed when dealing with very peripheral collisions. We have now introduced a variable $T = T(b)$ where b is the impact parameter of the collision. We argue that there are data which not only show that T must be a function of b but, in addition, also point to an approximate value of T for a given b. We propose a very simple formula: $T(b) = D_0 + D_1[A_s(b)/A_0]$ where $A_s(b)$ is the mass of the abraded PLF and A_0 is the mass of the projectile; D_0 and D_1 are constants. Using this model we compute cross sections for several collisions and compare with data.

DOI: 10.1103/PhysRevC.84.054612 PACS number(s): 25.70.Mn, 25.70.Pq

I. INTRODUCTION

In a recent paper [1] we proposed a model of projectile multifragmentation which was applied to collisions of Ni on Be and Ta at 140 MeV/nucleon and of Xe on Al at 790 MeV/nucleon. The model gave reasonable answers for most of the cross sections studied. The model requires integration over impact parameter. For a given impact parameter, the part of the projectile that does not directly overlap with the target is sheared off and defines the projectile-like fragment(PLF). This is abrasion and, appealing to the high energy of the beam, is calculated using straight line geometry. The PLF has N_s neutrons, Z_s protons, and A_s $(=N_s + Z_s)$ nucleons (the corresponding quantities for the full projectile are labeled N_0, Z_0, and A_0, respectively). The abraded system N_s, Z_s has a temperature. In the second stage, this hot PLF expands to one third of the normal nuclear density. Assuming statistical equilibrium, the breakup of the PLF at a temperature T is now calculated using the canonical thermodynamic model (CTM). The composites that result from this breakup have the same temperature T and can evolve further by sequential decay (evaporation). This is computed. Cross sections can now be compared with experiment. The agreements were reasonable except for very peripheral collisions and it was conjectured in Ref. [1] that the main reason for this discrepancy was due to the assumption of constant T over all impact parameters.

Full details are provided in Ref. [1]. Our aim here is to improve the model by incorporating an impact parameter dependence of $T = T(b)$. While we were led to this by computing the cross sections of very large PLFs (which can only result from very peripheral collisions), the effect of temperature dependence is accentuated in other experiments. In fact these experiments can be used, with some aid from reasonable models, to extract "experimental" values for temperature T at each b. We spend considerable time studying this, although our primary aim was and is the computation of cross sections from a theoretical model.

II. BASICS OF MODEL

Consider the abrasion stage. The projectile hits the target. Use straight line geometry. We can then calculate the volume of the projectile that goes into the participant region (Eqs. A.4.4 and A.4.5 of Ref. [2]). What remains in the PLF is V. This is a function of b. If the original volume of the projectile is V_0, the original number of neutrons is N_0, and the original number of protons is Z_0, then the average of neutrons in the PLF is $\langle N_s(b)\rangle = [V(b)/V_0]N_0$ and the average number of protons is $\langle Z_s(b)\rangle = [V(b)/V_0]Z_0$; $\langle N_s(b)\rangle$ [and similarly $\langle Z_s(b)\rangle$] is usually a noninteger. Since, in any event, only an integral number of neutrons (and protons) can appear in a PLF we need a prescription to get integral numbers. Let the two nearest integers to $\langle N_s(b)\rangle$ be $N_s^{\min}(b)$ and $N_s^{\max}(b) = N_s^{\min}(b) + 1$. We assume that $P_{N_s}(b)$, which is the probability that the abraded system has N_s neutrons, is zero unless $N_s(b)$ is either $N_s^{\min}(b)$ or $N_s^{\max}(b)$. Let $\langle N_s(b)\rangle = N_s^{\min}(b) + \alpha$ where α is less than 1. Then $P(N_s^{\max}(b)) = \alpha$ and $P(N_s^{\min}(b)) = 1 - \alpha$. Similar conditions apply to $P_{Z_s}(b)$. The probability that a PLF with N_s neutrons and Z_s protons materializes from a collision at impact parameter b is given by $P_{N_s,Z_s}(b) = P_{N_s}(b)P_{Z_s}(b)$. Once this PLF is formed it will expand and break up into composites at a temperature T. We use CTM to obtain these. All the relevant details of CTM can be found in Refs. [1] and [3]. We will not repeat these here. There can be very light fragments, intermediate-mass fragments (defined more precisely in the next section), and heavier fragments. As the fragments are at temperature T it is possible that some of these will sequentially decay, thereby changing the final population which is measured experimentally. Details of evaporation can be found in Refs. [1] and [4].

III. ARGUMENTS FOR b DEPENDENCE OF TEMPERATURE

Experimental data on $M_{\rm IMF}$ as a function of $Z_{\rm bound}$ (see Fig. 1 in [5]) Ref. probably provide the strongest arguments for

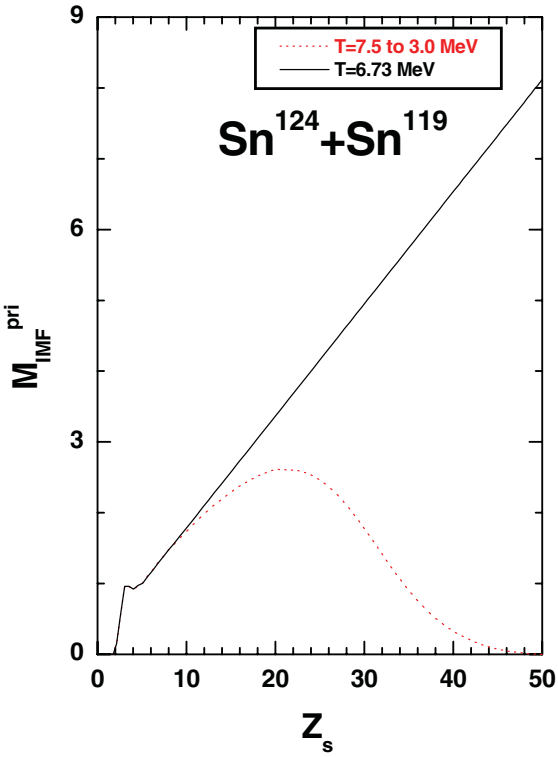

FIG. 1. (Color online) Mean multiplicity of intermediate-mass fragments $M_{\rm IMF}$ (after multifragmentation stage) as a function of projectile spectator charge for ^{124}Sn on ^{119}Sn reaction calculated at a fixed temperature $T = 6.73$ MeV (black solid line) and at a linearly decreasing temperature from 7.5 MeV at $b = 0$ to 3 MeV at $b_{\rm max}$ (red dotted line). The ordinate is labeled $M^{\rm pri}_{\rm IMF}$ because the effect of evaporation is not included.

needing an impact parameter dependence of the temperature. Here, $M_{\rm IMF}$ is the average multiplicity of intermediate-mass fragments (in this work, those with z between 3 and 20) and $Z_{\rm bound}$ is the sum of all charges coming from the PLF minus particles with $z = 1$. For ease of arguments we will neglect, in this section, the difference between $Z_{\rm bound}$ and Z_s, which is the total charge of all particles which originate from the PLF. A large value of $Z_{\rm bound}$ (close to Z_0 of the projectile) signifies that the PLF is large and the collision is peripheral (large b), whereas a relatively smaller value of $Z_{\rm bound}$ will imply a more central collision (small b). For an equal-mass collision, $Z_{\rm bound}$ goes from zero to Z_0, which is the total charge of the projectile.

The following gross features of heavy-ion collisions at intermediate energy are known. If the excitation energy (or the temperature) of the dissociating system is low then one large fragment and a small number of very light fragments emerge. The average multiplicity of intermediate-mass fragments (IMFs) is very small. As the temperature increases, very light as well as intermediate-mass fragments appear at the expense of the heavy fragment. The multiplicity $M_{\rm IMF}$ will grow as a function of temperature, will reach a peak, and then begin to go down as, at a high temperature, only light particles are dominant. For evidence and discussion of this see [6].

For projectile fragmentation, we are in the domain where $M_{\rm IMF}$ rises with temperature. Now, at constant temperature, let us consider what must happen if the dissociating system grows bigger. We expect $M_{\rm IMF}$ will increase with the size of the dissociating system; that is, with $Z_{\rm bound}$. Experimental data are quite different: $M_{\rm IMF}$ initially increases, reaches a maximum at a particular value of $Z_{\rm bound}$, and then goes down.

In Fig. 1 we show two graphs for $M_{\rm IMF}$, one in which the temperature is kept fixed (at 6.73 MeV) and another in which T decreases linearly from 7.5 MeV (at $b = 0$) to 3 MeV at $b_{\rm max}$. The calculation is qualitative. The case considered is ^{124}Sn on ^{119}Sn. CTM is used to calculate $M_{\rm IMF}$ but evaporation is not included. Similarly, $Z_{\rm bound}$ is Z_s (no correction for $z = 1$ particles). Fuller calculations will be shown later, but the principal effects are all in the graphs. Keeping the temperature fixed makes $M_{\rm IMF}$ go up all the way until $Z_{\rm bound} = Z_0$ is reached. One needs the temperature to go down to bring down the value of $M_{\rm IMF}$ as seen in experiment.

IV. USE MODEL TO EXTRACT *b* DEPENDENCE OF TEMPERATURE

In our model we can use an iterative technique to deduce a temperature from experimental data of $M_{\rm IMF}$ vs $Z_{\rm bound}$. Pick a b; abrasion gives a $\langle Z_s \rangle$. Guess a temperature T. A full calculation with CTM and evaporation is now done to get a $Z_{\rm bound}$ and $M_{\rm IMF}$. This $Z_{\rm bound}$ will be close to $\langle Z_s \rangle$. If the guessed value of temperature is too low then the calculated value of $M_{\rm IMF}$ will be too little for this value of $Z_{\rm bound}$ when confronted with data. In the next iteration, the temperature will be raised. If, on the other hand, for the guessed value of T, the calculated $M_{\rm IMF}$ is too high, in the next iteration the temperature will be lowered. Of course when we change T, the calculated $Z_{\rm bound}$ will also shift, but this change is smaller and, with a small number of iterations, one can approximately reproduce an experimental pair $Z_{\rm bound}$, $M_{\rm IMF}$.

For the case of ^{124}Sn on ^{119}Sn, we provide Table I which demonstrates this. The first two columns are from experiment [7]. The numbers used in the table were given to us by Trautmann. The next two columns are the values of $Z_{\rm bound}$ and $M_{\rm IMF}$ that we get from our iterative procedure. These values are taken to be close enough to the experimental pair. These are obtained for a value of b (sixth column) and a temperature T (fifth column). Table II provides a similar compilation for ^{107}Sn on ^{119}Sn.

Having deduced once for all such "experimental data" of T vs b, one can try simple parametrization like $T(b) = C_0 + C_1 b + C_2 b^2 + \cdots$ and see how well they fit the data. We show this for the two cases in Fig. 2.

In Fig. 3, by using such parametrized versions of T, we compute $M_{\rm IMF}$ vs $Z_{\rm bound}$ and compare with experimental data. Except for fluctuations in the values of $M_{\rm IMF}$ for very low values of $Z_{\rm bound}$, the fits are very good. We will return to the cases of fluctuations in a later section.

TABLE I. Best-fit and experimental values for ^{124}Sn on ^{119}Sn. The first two columns are data from experiment [7]. The next two columns are the values of $Z_{\rm bound}$ and $M_{\rm IMF}$ we get from our iterative procedure. These values are taken to be close enough to the experimental pair. These are obtained for a value of b (fifth column) and a temperature T (sixth column).

Experimental		Theoretical			
$Z_{\rm bound}$	$M_{\rm IMF}$	$Z_{\rm bound}$	$M_{\rm IMF}$	b (fm)	Required T (MeV)
11.0	1.421	11.080	1.424	2.912	6.398
15.0	1.825	15.094	1.818	3.625	6.108
20.0	2.145	19.984	2.131	4.4574	5.840
25.0	2.010	25.024	2.019	5.289	5.520
30.0	1.505	29.854	1.545	6.122	5.250
35.0	0.920	34.985	0.928	7.072	4.970
40.0	0.415	39.639	0.424	8.023	4.650
45.0	0.193	44.763	0.196	9.331	4.350
47.0	0.156	46.512	0.154	9.925	4.260
49.0	0.135	48.425	0.130	10.876	4.190

V. TEMPERATURES EXTRACTED FROM ISOTOPE POPULATIONS

In the preceding sections we extracted temperatures T (combining data and model) at values of b (equivalently at values of $Z_{\rm bound}$). This is a different method for extracting temperature. A more standard way of extracting temperatures is the Albergo formula [8], which has been widely used in the past (for a review see, for example, [9,10]). In Ref. [7], Figs. 24 and 25, temperatures at selected values of $Z_{\rm bound}/Z_0$ were extracted from populations in [^{3,4}He,^{6,7}Li] and [^{7,9}Be,^{6,8}Li] using the Albergo formula. These temperatures are compared in Fig. 4 with a typical temperature profile deduced here. It is gratifying to see that such different methods of of extraction give very good agreement except at very low values of b (i.e., small value of $Z_{\rm bound}$). We do not know why the results begin to differ at low values of b.

TABLE II. Same as Table 1, except that here the projectile is ^{107}Sn instead of ^{124}Sn.

Experimental		Theoretical			
$Z_{\rm bound}$	$M_{\rm IMF}$	$Z_{\rm bound}$	$M_{\rm IMF}$	b (fm)	Required T (MeV)
15.0	1.690	14.816	1.583	3.886	6.200
20.0	1.923	19.865	1.906	4.698	5.740
21.0	1.984	21.207	1.976	4.930	5.705
25.0	1.749	24.913	1.758	5.510	5.320
30.0	1.079	30.356	1.075	6.438	4.900
35.0	0.581	35.252	0.602	7.366	4.600
40.0	0.223	40.123	0.225	8.410	4.210
45.0	0.201	44.676	0.199	9.802	4.100
47.0	0.201	47024	0.159	10.876	4.000

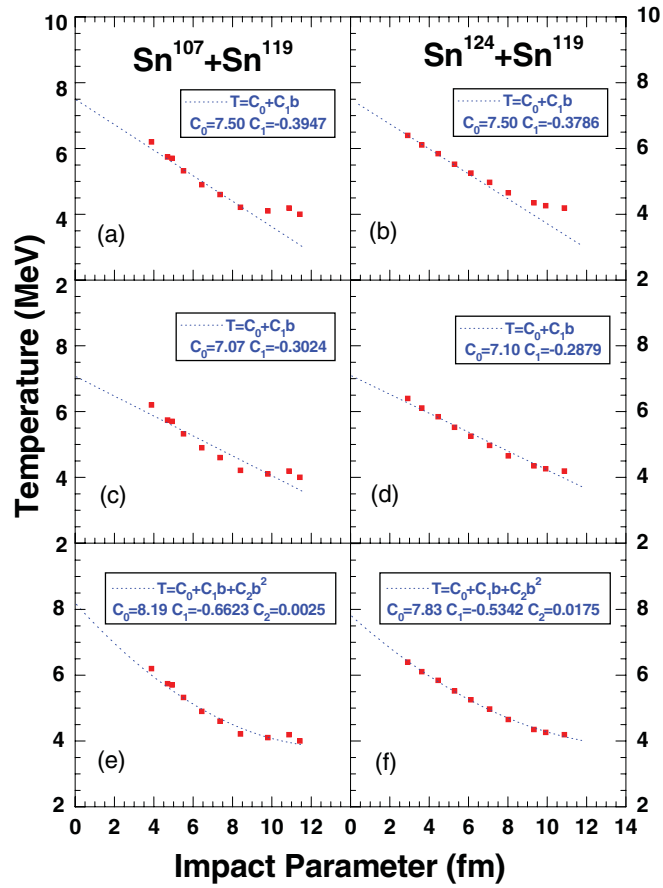

FIG. 2. (Color online) Impact parameter dependence of temperature for ^{107}Sn on ^{119}Sn [(a), (c) and (e)] and ^{124}Sn on ^{119}Sn reactions [(b), (d), and (f)]. In (a) and (b), the red squares represent the extracted temperatures (sixth column of Tables I and II) and the blue dotted lines are the linearly decreasing temperature profile from 7.5 to 3 MeV. The blue dotted lines of middle panels [(c) and (d)] and lower panels [(e) and (f)] represent fitting of extracted temperatures (red squares) with $T(b) = C_0 + C_1 b$ and $T(b) = C_0 + C_1 b + C_2 b^2$, respectively. The unit of C_0 is MeV, C_1 is MeV/fm and C_2 is MeV/fm^2.

VI. FLUCTUATIONS IN $M_{\rm IMF}$ FOR SMALL $Z_{\rm bound}$

For small values of $Z_{\rm bound}$ the measured $M_{\rm IMF}$ shows considerable fluctuations as we go from one value of $Z_{\rm bound}$ to another (see Fig. 3). Our model does not reproduce these although the general shapes are correct. Statistical models are not expected to show such fluctuations, but let us get into some detail which (a) give a clue how such fluctuations may arise and (b) why our model misses them. The reader who is not interested in such details can skip the rest of this section without loss of continuity.

We first indicate how such fluctuations may arise in experiments and then explain why the model used here misses them. One can use some very general arguments to prove that, by the very nature of the cuts imposed in the experiment (i.e., in each event, $Z_{\rm bound} = Z_s$ minus charges of all composites with charge $z = 1$ and IMF = composites with charge z from 3 to 20), $M_{\rm IMF}$ will be 1 for $Z_{\rm bound} = 3$ or 5 whereas for $Z_{\rm bound} = 4$, $M_{\rm IMF}$ will be very small. Apart from the cuts imposed in the experiment this also depends on nuclear structure: that there are

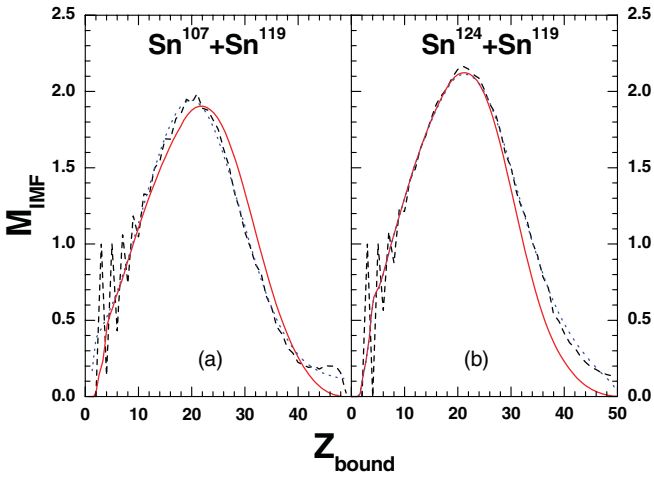

FIG. 3. (Color online) Mean multiplicity of intermediate-mass fragments $M_{\rm IMF}$, as a function of $Z_{\rm bound}$ for (a) ^{107}Sn on ^{119}Sn and (b) ^{124}Sn on ^{119}Sn reactions calculated using linearly decreasing temperature from 7.5 to 3 MeV (red solid lines) and $T(b) = C_0 + C_1 b + C_2 b^2$ profile (blue dotted lines). The experimental results [7] are shown by the black dashed lines.

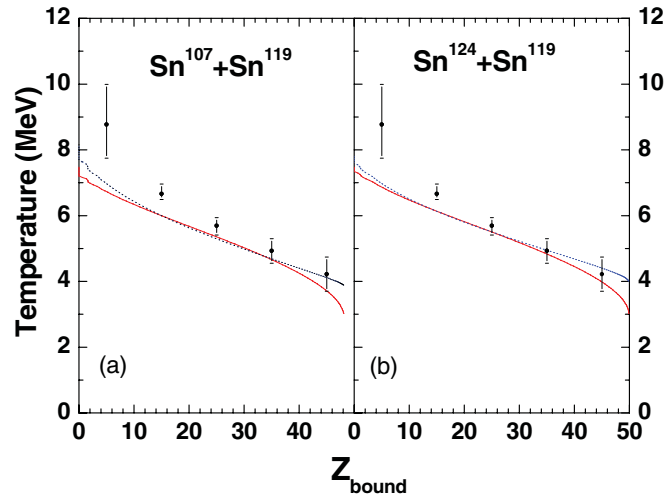

FIG. 4. (Color online) Comparison of theoretically used temperature profiles (i) temperature decreasing linearly with impact parameter from 7.5 to 3 MeV (red solid lines), (ii) $T(b) = C_0 + C_1 b + C_2 b^2$ fitting temperature (blue dotted lines) with that deduced by Albergo formula from experimental data [7] (black points with error bars) for (a) ^{107}Sn on ^{119}Sn and (b) ^{124}Sn on ^{119}Sn.

particle stable states in Li and B, but all states in ^{8}Be and many states in other Be isotopes are fragile against emitting two $^{4}_{2}$He.

Now we explain why the experimental data on fluctuations in $M_{\rm IMF}$ seen in very small systems are not reproduced in the model pursued here. There are two reasons for this. One is that our calculation does not map very well to the experimental situation. Experimentally, $Z_{\rm bound}$ is found event by event. It is an integer and, for the same value of $Z_{\rm bound}$, the average value $M_{\rm IMF}$ is determined and tabulated. In the calculation done here, we consider $Z_{\rm bound}$ to be given by $Z_s - \sum_i n_{z=1}(i)$ where $n_{z=1}(i)$ stands for the average multiplicity of proton or deuteron or triton. In our calculation, although Z_s is an integer, $Z_{\rm bound}$ is not since the $n_{z=1}(i)$ values (average number of composites i) are not. What we are obtaining here is an average of $M_{\rm IMF}$ done over $M_{\rm IMF}$ belonging to different but neighboring values of integral $Z_{\rm bound}$. This would be quite wrong if the values of $M_{\rm IMF}$ belonging to neighboring values of $Z_{\rm bound}$ differ greatly (as happens for very small systems) but, for large systems, the difference would be small and our prescription is adequate for an estimate.

The other weakness of our calculation is the use of the liquid-drop model for the ground-state energy and the Fermi-gas model for energies of excited states for such small nuclei.

For very small PLFs, it is possible to keep the main ingredients of our model: abrasion, followed by expansion and disintegration by CTM, followed by decay of CTM products using realistic energy levels and branching properties from nuclear structure data. We hope to present such results for Z_s up to 6 soon. For larger systems the procedure gets quickly very complicated but past experience shows that, for larger systems, the methods used here are adequate.

Figure 7 in Ref. [7] shows that statistical multifragmentation model (SMM) calculations are able to reproduce the fluctuations faithfully. Actually, in those calculations the occurrences of Z_s, N_s with associated E_x are not calculated but guessed so that the ensemble produces the data as faithfully as possible. For further details how these calculations were done please refer to Ref. [11].

VII. TOWARDS A UNIVERSAL TEMPERATURE PROFILE

Knowing the temperature profile $T = T(b)$ in one case (say, ^{124}Sn on ^{119}Sn), can we anticipate what $T = T(b)$ will be like in another case (say, ^{58}Ni on ^{9}Be)? In both the cases $b_{\rm min}$ is zero and $b_{\rm max}$ is $R_1 + R_2$ yet we cannot expect the same functional form $T = T(b/b_{\rm max})$ for both the cases. In the first case, near $b = 0$, a small change in b causes a large fractional change in the mass of the PLF whereas, for ^{58}Ni on ^{9}Be and near $b = 0$, a small change in b causes very little change in the mass of the PLF. Thus, we might expect the temperature to change more rapidly in the first case near $b = 0$ whereas, in the second case, the temperature may change very little since not much changed when b changed a little. In fact, for Ni on Be, transport model calculations (heavy-ion phase space exploration, or HIPSE, and antisymmetrized molecular dynamics, or AMD) find that, starting from $b = 0$, excitation energy per particle changes very little in the beginning [12]. In terms of our model, this would mean that, for Ni on Be, T would be slow to change in the beginning.

We might argue that a measure of the wound that the projectile suffers in a heavy-ion collision is $1.0 - A_s/A_0$ and that the temperature depends upon the wound. Thus, we should expect $T = T[A_s(b)/A_0]$. Just as we can write $T(b) = C_0 + C_1 b + C_2 b^2 + \cdots$ so also we could expand in powers of $A_s(b)/A_0$, [i.e., $T(b) = D_0 + D_1[A_s(b)/A_0] + D_2[A_s(b)/A_0]^2 + \cdots$]. We try such fits to the "experimental" temperature profile given in Tables I and II. From b we deduce $A_s(b)/A_0$ and plot T as a function of $A_s(b)/A_0$. A linear fit appears to be good enough (Fig. 5).

The specification that $T(b) = D_0 + D_1[A_s(b)/A_0]$ has profound consequences. This means the temperature profile $T(b/b_{\max})$ of ^{124}Sn on ^{119}Sn is very different from that of ^{58}Ni on ^{9}Be. In the first case, $A_s(b)/A_0$ is nearly zero for $b = b_{\min} = 0$ whereas, in the latter case, $A_s(b)/A_0 \approx 0.6$ for $b = b_{\min} = 0$. For $D_0 = 7.5$ MeV and $D_1 = -4.5$ MeV, the temperature profiles are compared in Fig. 6. An even more remarkable feature is that the temperature profile of ^{58}Ni on ^{9}Be is so different from the temperature profile of ^{58}Ni on ^{181}Ta. In the latter case $b_{\min} = R_{\rm Ta} - R_{\rm Ni}$ and beyond $b_{\min}$, $A_s(b)/A_0$ grows from zero to 1 for $b_{\max}$. This is very similar to the temperature profile of ^{124}Sn on ^{119}Sn.

VIII. FORMULAE FOR CROSS SECTIONS

Now that we have established that temperature T should be considered impact-parameter (b) dependent, let us write down how cross sections should be evaluated. We first start with abrasion cross section. In Eq. (1) of Ref. [1], the abrasion cross section was written as

$$\sigma_{a,N_s,Z_s} = 2\pi \int bdb\, P_{N_s,Z_s}(b), \qquad (1)$$

where $P_{N_s,Z_s}(b)$ is the probability that a PLF with N_s neutrons and Z_s protons emerges in collision at impact parameter b. Actually, there is an extra parameter that needs to be specified. The complete labeling is $\sigma_{a,N_s,Z_s,T}$ if we assume that, irrespective of the value of b, the PLF has a temperature T. Here we have broadened this to the more general case where the temperature is dependent on the impact parameter b. Thus the PLF with N_s neutrons and Z_s protons will be formed in a small range of temperature (because the production of a particular N_s, Z_s occurs in a small range of b).

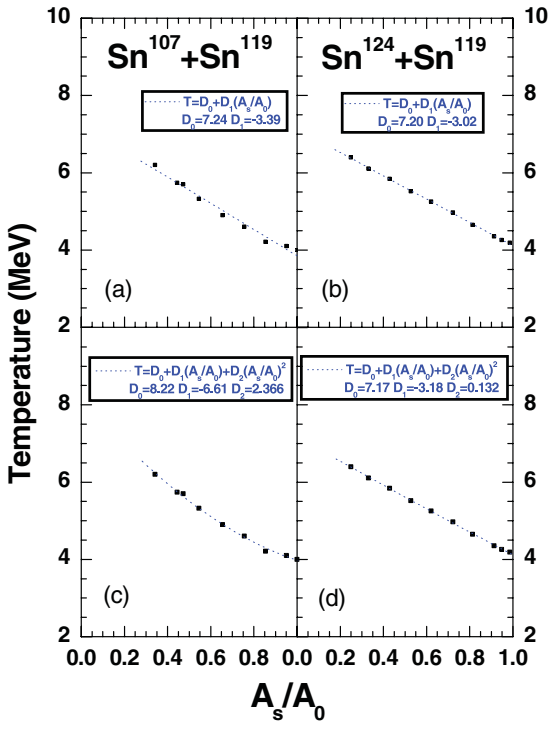

FIG. 5. (Color online) Fitting of extracted temperatures (red squares) with $T(b) = D_0 + D_1[A_s(b)/A_0]$ [blue dotted lines in (a) and (b)] and $T(b) = D_0 + D_1[A_s(b)/A_0] + D_2[A_s(b)/A_0]^2$ profile [blue dotted lines in (c) and (d)] for ^{107}Sn on ^{119}Sn [(a) and (c)] and ^{124}Sn on ^{119}Sn [(b) and (d)]. The units of D_0, D_1, and D_2 are MeV.

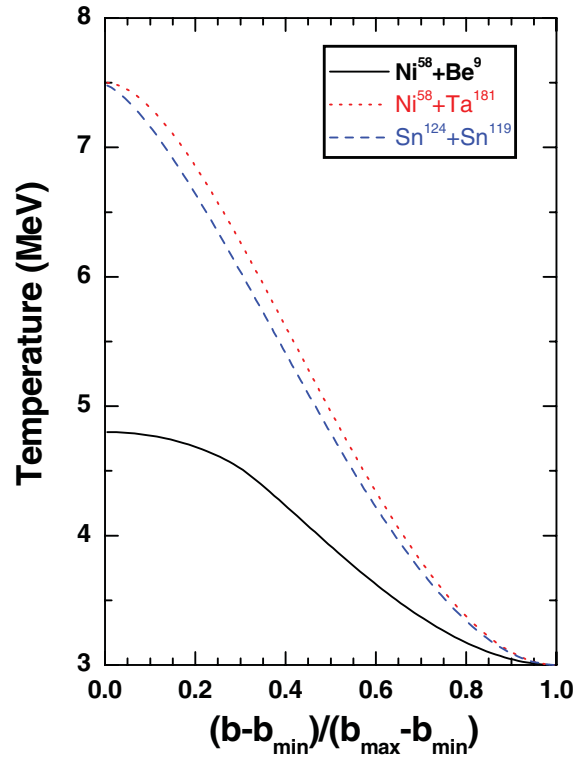

FIG. 6. (Color online) Temperature profile for ^{58}Ni on ^{9}Be (black solid line), ^{58}Ni on ^{181}Ta (red dotted line), and ^{124}Sn on ^{119}Sn (blue dashed line) by considering $T = [7.5 - 4.5[A_s(b)/A_0]]$ MeV.

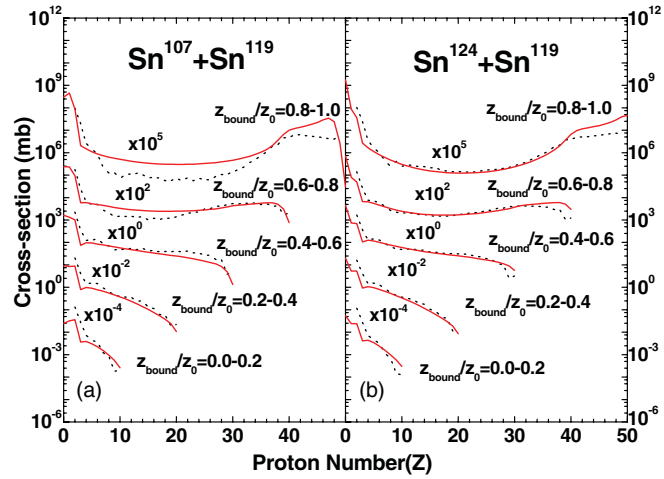

FIG. 7. (Color online) Theoretical total charge cross-section distribution (red solid lines) for (a) ^{107}Sn on ^{119}Sn and (b) ^{124}Sn on ^{119}Sn reactions sorted into five intervals of $Z_{\rm bound}/Z_0$ ranging between 0.0 to 0.2, 0.2 to 0.4, 0.4 to 0.6, 0.6 to 0.8, and 0.8 to 1.0 with different multiplicative factors 10^{-4}, 10^{-2}, 10^{0}, 10^{2}, and 10^{5}, respectively. The experimental data Ref. [7] are shown by black dashed lines. The theoretical calculation is done using linearly decreasing temperature from 7.5 MeV at $b = 0$ to 3 MeV at $b_{\max}$.

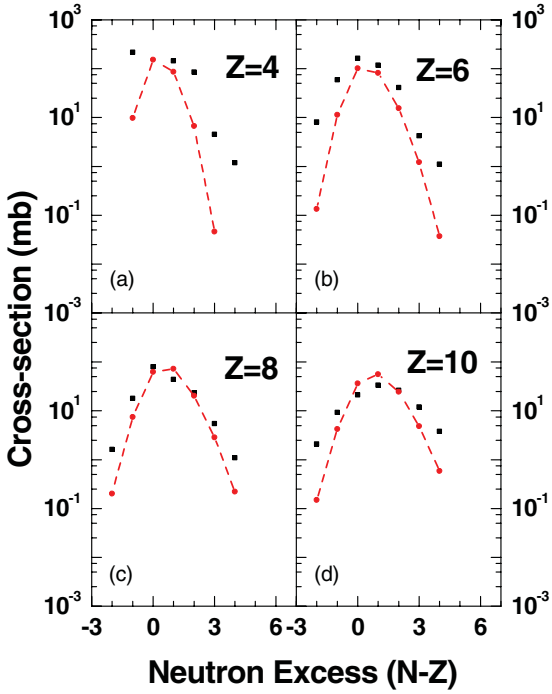

FIG. 8. (Color online) Theoretical isotopic cross-section distribution (circles joined by dashed lines) for ^{107}Sn on ^{119}Sn reaction summed over $0.2 \leqslant Z_{\rm bound}/Z_0 \leqslant 0.8$. The experimental data [7] are shown by black squares. Theoretical calculation is done using linearly decreasing temperature from 7.5 MeV at $b = 0$ to 3 MeV at $b_{\rm max}$.

To proceed, let us discretize. We divide the interval $b_{\rm min}$ to $b_{\rm max}$ into small segments of length Δb. Let the midpoint of the ith bin be $\langle b_i \rangle$ and the temperature for collision at $\langle b_i \rangle$ be T_i.

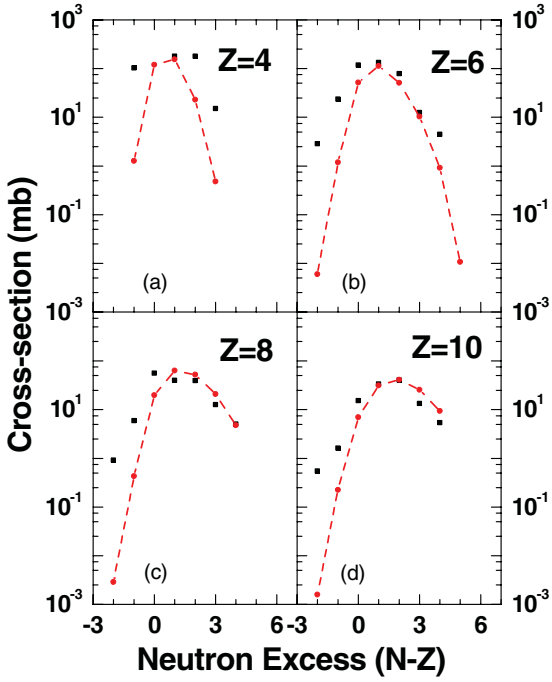

FIG. 9. (Color online) Same as Fig. 8, except that here the projectile is ^{124}Sn instead of ^{107}Sn.

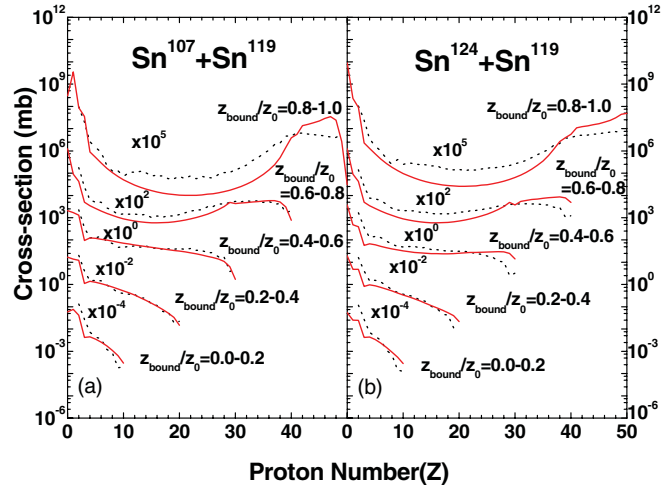

FIG. 10. (Color online) Same as Fig. 7 except that here the temperature profile is $T(b) = 7.5$ MeV $- [A_s(b)/A_0]4.5$ MeV instead of linearly decreasing temperature from 7.5 MeV at $b = 0$ to 3 MeV at $b_{\rm max}$.

Then

$$\sigma_{a,N_s,Z_s} = \sum_i \sigma_{a,N_s,Z_s,T_i}, \tag{2}$$

where

$$\sigma_{a,N_s,Z_s,T_i} = 2\pi \langle b_i \rangle \Delta b P_{N_s,Z_s}(\langle b_i \rangle) \tag{3}$$

PLFs with the same N_s, Z_s but different T_i are treated independently. The rest of the calculation proceeds as in Ref. [1]. If, after abrasion, we have a system N_s, Z_s at temperature T_i, the CTM allows us to compute the average

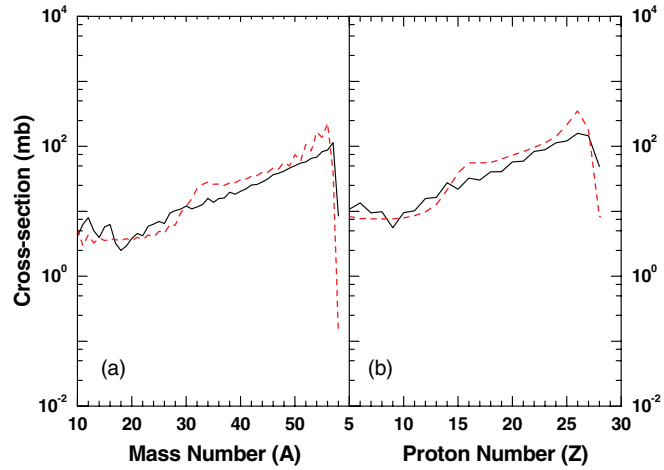

FIG. 11. (Color online) (a) Total mass and (b) total charge cross-section distribution for the ^{58}Ni on ^{9}Be reaction. The left panel shows the cross sections as a function of the mass number, while the right panel displays the cross sections as a function of the proton number. The theoretical calculation is done using temperature decreasing linearly with A_s/A_0 from 7.5 to 3.0 MeV (dashed line) and compared with the experimental data [14] (solid line).

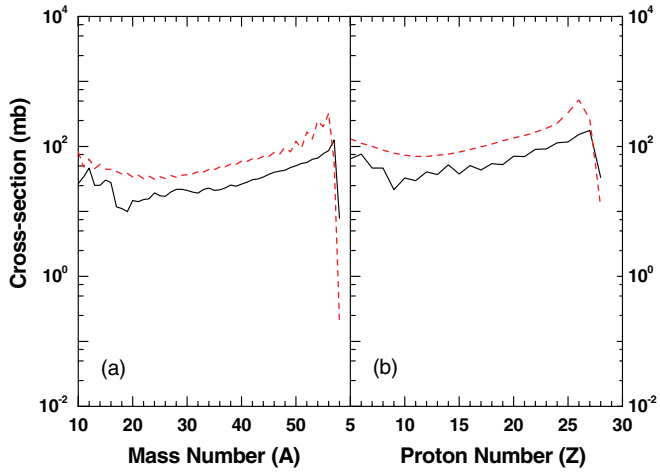

FIG. 12. (Color online) Same as Fig. 11 except that here the target is ^{181}Ta instead of ^{9}Be.

population of the composite with neutron number n and proton number z when this system breaks up (this composite is at temperature T_i). Denote this by $M_{n,z}^{N_s,Z_s,T_i}$. It then follows, summing over all the abraded N_s, Z_s that can yield n, z that the primary cross section for n, z is

$$\sigma_{n,z}^{\mathrm{pr}} = \sum_{N_s,Z_s,T_i} M_{n,z}^{N_s,Z_s,T_i} \sigma_{a,N_s,Z_s,T_i}. \tag{4}$$

Finally, evaporation from these composites n, z at temperatures T_i is considered before comparing with experimental data.

IX. CROSS SECTIONS FOR DIFFERENT REACTIONS

We will now show some results for cross sections using our model and compare with experimental data. We first show results for ^{124}Sn on ^{119}Sn and ^{107}Sn on ^{119}Sn at 600 MeV/nucleon beam energy. The experimental data are plotted in [7] and the data were given to us by Trautmann. The differential charge distributions and isotopic distributions for ^{107}Sn on ^{119}Sn and ^{124}Sn on ^{119}Sn were theoretically calculated using $T(b) = C_0 + C_1 b$ and and also $T(b) = D_0 + D_1[A_s(b)/A_0]$. So long as the temperature values at the two endpoints of b are the same, the answers did not differ much. In Fig. 7 we have shown results for T varying linearly with b with $T_{\max} = 7.5$ MeV and $T_{\min} = 3$ MeV. At each Z_{bound}, the charge distribution and isotopic distributions are calculated separately and finally integrated over different Z_{bound} ranges. The differential charge distributions are shown in Fig. 7 for different intervals of Z_{bound}/Z_0 ranging between 0.0 to 0.2, 0.2 to 0.4, 0.4 to 0.6, 0.6 to 0.8, and 0.8 to 1.0. For the sake of clarity the distributions are normalized with different multiplicative factors. At peripheral collisions (i.e., $0.8 \leqslant Z_{\mathrm{bound}}/Z_0 \leqslant 1.0$) due to the small temperature of the projectile spectator, it breaks into one large fragment and a small number of light fragments; hence the charge distribution shows a U-type nature. But with the decrease of impact parameter the temperature increases, the projectile spectator breaks into large number of fragments, and the charge distributions become steeper. In Figs. 8 and 9 the integrated isotopic distributions over the range $0.2 \leqslant Z_{\mathrm{bound}}/Z_0 \leqslant 0.8$ for beryllium, carbon, oxygen, and neon are plotted and compared with the experimental result for the ^{107}Sn on ^{119}Sn and ^{124}Sn on ^{119}Sn reactions, respectively.

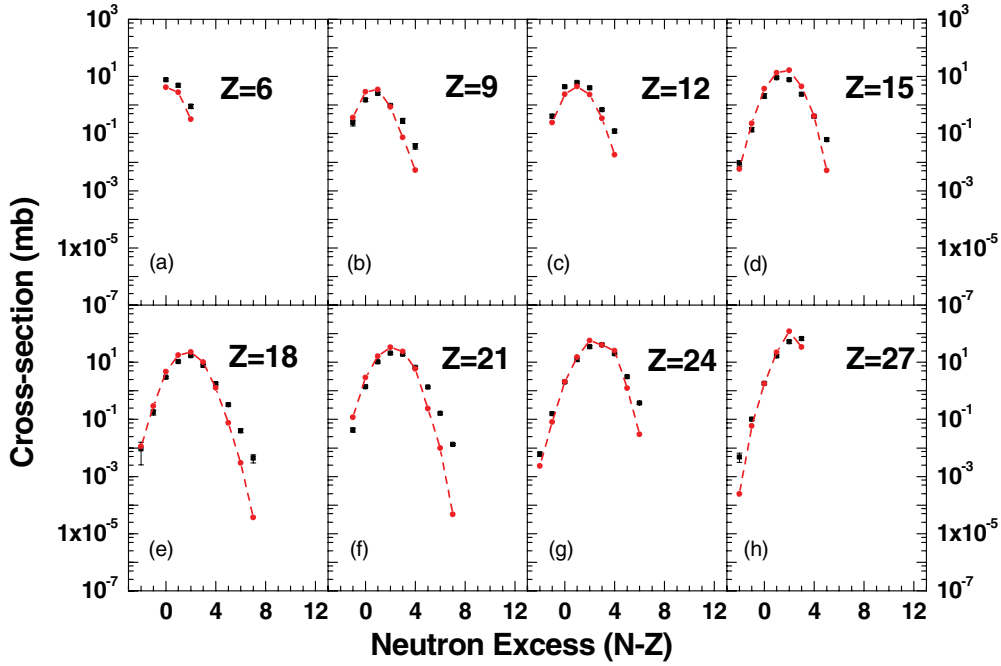

FIG. 13. (Color online) Theoretical isotopic cross-section distribution (circles joined by dashed lines) for ^{58}Ni on ^{9}Be reaction compared with experimental data [14] (squares with error bars).

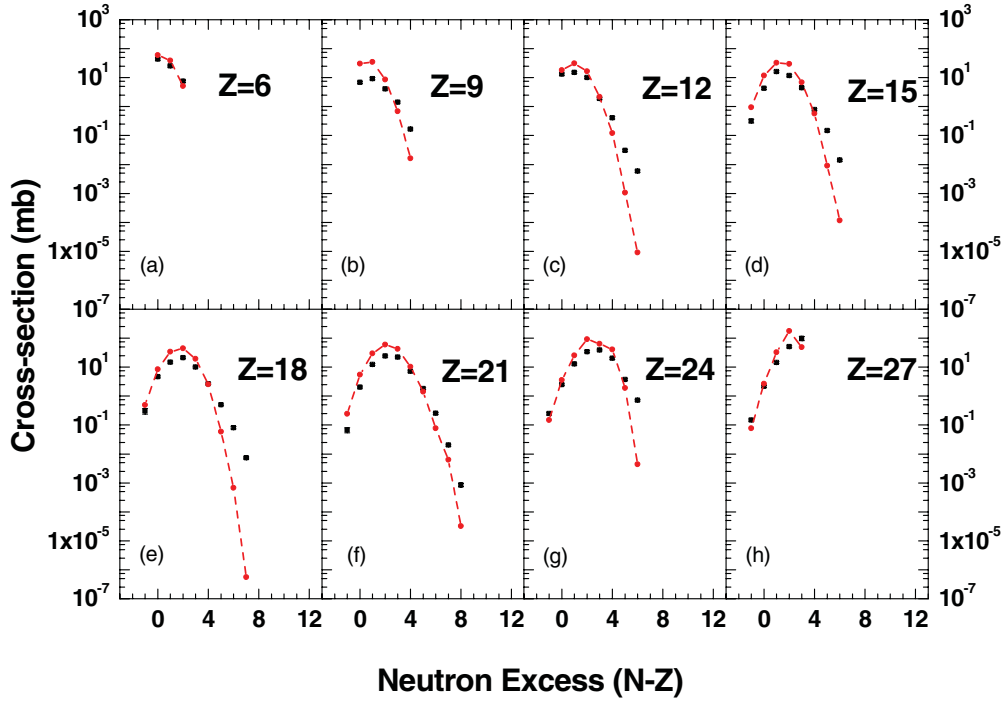

FIG. 14. (Color online) Same as Fig. 13 except that here the target is ^{181}Ta instead of ^{9}Be.

The rest of the cross sections shown all use $T(b) = 7.5\ \text{MeV} - [A_S(b)/A_0]4.5\ \text{MeV}$. First, in Fig. 10 the calculations of Fig. 7 are redone but with the above parametrization. Next, we look at data for ^{58}Ni on ^{9}Be and ^{181}Ta at a beam energy of 140 MeV/nucleon done at Michigan State University. The data were made available to us by Mocko [14]. Calculations were also done with ^{64}Ni as the beam. Those results agree with experiment equally well but are not shown here for brevity. The results for ^{58}Ni on ^{9}Be and ^{58}Ni on ^{181}Ta are shown in

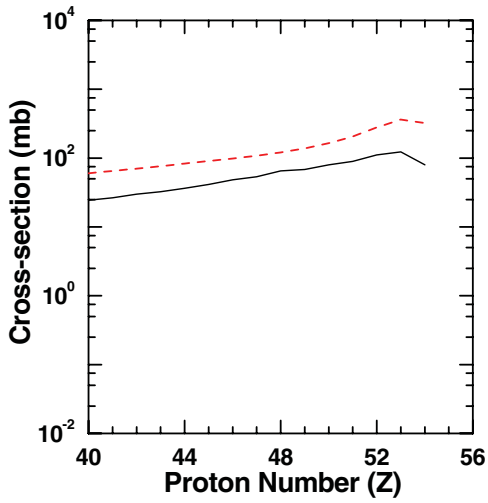

FIG. 15. (Color online) Total charge cross-section distribution for the ^{129}Xe on ^{27}Al reaction. The theoretical calculation is done using temperature decreasing linearly with A_s/A_0 from 7.5 to 3.0 MeV (dashed line) and compared with the experimental data [13] (solid line).

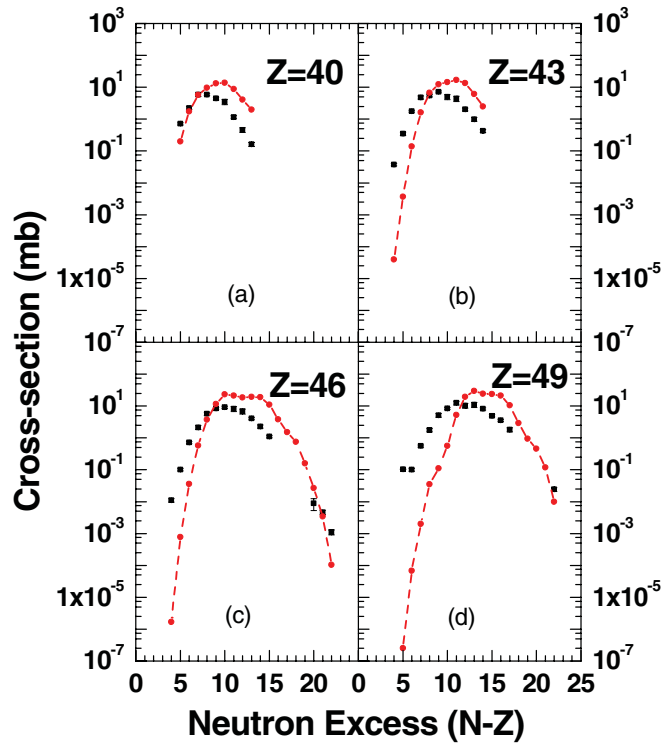

FIG. 16. (Color online) Theoretical isotopic cross-section distribution (circles joined by dashed lines) for ^{129}Xe on ^{27}Al reaction compared with experimental data [13] (squares with error bars).

Figs. 11 to 14. The experimental data are from Ref. [12]. The chief difference from results shown in Refs. [1] is that we are able to include data for very peripheral collisions. Next we look at some older data from ^{129}Xe on ^{27}Al at 790 MeV/nucleon [13]. Results are given in Figs. 15 and 16.

The parametrization $T(b) = 7.5$ MeV $- [A_s(b)/A_0]$ 4.5 MeV was arrived at by trying to fit many reaction-cross-section data. A better fit for $M_{\rm IMF}$ vs $Z_{\rm bound}$ for Sn isotopes is found with slightly different values: $T(b) = 7.2$ MeV $- [A_s(b)/A_0]3.2$ MeV.

Lastly, we comment on some shortcomings of the calculations reported here. Looking at Figs. 8, 9, 13, and 14, the widths of the cross sections as functions of neutron excess appear to be slightly narrower than what is seen in experiments. Since this appears to be a universal pattern one would hope to have a general cure for this. Previous calculations on this aspect [7] suggest that reducing the symmetry energy in the liquid-drop formula improves this. We have not investigated this in our model but this and other related issues like isoscaling will be investigated in the future. We also point out that fits for ^{129}Xe on ^{27}Al (Fig. 16) are of lower quality than those for Ni and Sn projectiles. Results would improve here with slightly augmented temperatures but we wanted to see how well one can do with one universal temperature profile without any adjustments.

X. SUMMARY AND DISCUSSION

We have shown that there are specific experimental data in projectile fragmentation which clearly establish the need to introduce an impact parameter dependence of temperature T in the PLF formed. Combining data and a model one can establish approximate values of $T = T(b)$. The model for cross sections has been extended to incorporate this temperature variation. This has allowed us to investigate more peripheral collisions. In addition, the impact parameter dependence of temperature appears to be very simple: $T(b) = D_0 + D_1[A_s(b)/A_0]$ where D_0 and D_1 are constants, $A_s(b)$ is the mass of the PLF, and A_0 is the mass of the projectile. With this model, we plan to embark upon an exhaustive study of available data on projectile fragmentation.

ACKNOWLEDGMENTS

This work was supported in part by Natural Sciences and Engineering Research Council of Canada. The authors are thankful to Professor Wolfgang Trautmann and Dr. M. Mocko for access to experimental data. S. Mallik is thankful for a very productive and enjoyable stay at McGill University for part of this work. S. Das Gupta thanks Dr. Santanu Pal for hospitality at Variable Energy Cyclotron Centre at Kolkata.

[1] S. Mallik, G. Chaudhuri, and S. Das Gupta, Phys. Rev. C **83**, 044612 (2011).
[2] S. Das Gupta and A. Z. Mekjian, Phys. Rep. **72**, 131 (1981).
[3] C. B. Das, S. Das Gupta, W. G. Lynch, A. Z. Mekjian, and M. B. Tsang, Phys. Rep. **406**, 1 (2005).
[4] G. Chaudhuri and S. Mallik, Nucl. Phys. A **849**, 190 (2011).
[5] C. Sfienti *et al.*, Phys. Rev. Lett. **102**, 152701 (2009).
[6] M. B. Tsang *et al.*, Phys. Rev. Lett. **71**, 1502 (1993).
[7] R. Ogul *et al.*, Phys. Rev. C **83**, 024608 (2011).
[8] S. Albergo, S. Costa, E. Costanzo, and A. Rubbino, Nuovo Cimento A **89**, 1 (1985).
[9] S. Das Gupta, A. Z. Mekjian, and M. B. Tsang (edited by J. W. Negele and E. Vogt, Plenum Publishers, New York), Adv. Nucl. Phys. **26**, 89 (2001).
[10] J. Pochodzalla and W. Trautmann, in *Isospin Physics in Heavy-Ion Collisions at Intermediate Energies*, edited by B.-A. Li and W. U. Schröder (Nova Science Publishers, Inc., Huntington, 2001), pg. 451.
[11] A. S. Botvina *et al.*, Nucl. Phys. A **584**, 737 (1995).
[12] M. Mocko, M. B. Tsang, D. Lacroix, A. Ono, P. Danielewicz, W. G. Lynch, and R. J. Charity, Phys. Rev. C **78**, 024612 (2008).
[13] J. Reinhold *et al.*, Phys. Rev. C **58**, 247 (1998).
[14] M. Mocko, Ph.D. thesis (unpublished), Michigan State University, 2006.